Modification of semiconductor or metal nanoparticle lattices in amorphous alumina by MeV heavy ions

New Journal of Physics

The open access journal at the forefront of physics

CrossMark

PAPER

OPEN ACCESS

Modification of semiconductor or metal nanoparticle lattices in amorphous alumina by MeV heavy ions

I Bogdanović Radović[1], M Buljan[1], M Karlušić[1], M Jerčinović[1], G Dražić[2], S Bernstorff[3] and R Boettger[4]

1 Ruđer Bošković Institute, Bijenička cesta 54, 10000 Zagreb, Croatia
2 National Institute of Chemistry, Ljubljana, Slovenia
3 Elettra-Sincrotrone Trieste, SS 14, km 163.5, I-34149 Basovizza (TS), Italy
4 Helmholtz-Zentrum Dresden-Rossendorf, Dresden, Germany

E-mail: iva@irb.hr

Abstract

In the present work we investigate effects of MeV heavy ions (from 0.4 MeV Xe to 15 MeV Si) on regularly ordered nanoparticle (NP) lattices embedded in amorphous alumina matrix. These nanostructures were produced by self-assembling growth using magnetron-sputtering deposition. From grazing incidence small-angle x-ray scattering measurements we have found that the used MeV heavy ions do not change the NP sizes, shapes or distances among them. However, ions cause a tilt of the entire NP lattice in the direction parallel to the surface. The tilt angle depends on the incident ion energy, type and the applied fluence and a nearly linear increase of the tilt angle with the ion fluence and irradiation angle was found. This way, MeV heavy ion irradiation can be used to design custom-made NP lattices. In addition, grazing incidence small-angle x-ray scattering can be effectively used as a method for the determination of material redistribution/shift caused by the ion hammering effect. For the first time, the deformation yield in amorphous alumina was determined for irradiation performed at the room temperature.

1. Introduction

Materials consisting of metal or semiconductor nanoparticles (NPs) are very interesting for many applications, especially in the field of photonics (lasers, sensors, photovoltaic devices, imaging, data storage, etc) [1–4]. Properties of such materials depend strongly on the NP size and arrangement and therefore it is very important to control the production of such materials. Many authors have studied the effects of ion beam irradiation on NPs embedded in amorphous matrix. It was found that if metal NPs embedded in amorphous silica are irradiated with swift heavy ions (SHIs) they may undergo a shape transformation from spherical to rod-like shape with the elongation direction aligned along that of the incident ions. It was also observed that spherical NPs below a minimum diameter (4–7 nm) remained spherical under SHI irradiation but progressively decreased in size as a result of dissolution into the SiO_2 matrix [5]. Previous studies of crystalline Ge NPs embedded in silica have shown that SHIs can modify them in different ways. Depending on the SHI electronic stopping power (S_e), ion fluence and initial NP size, Ge NPs can elongate along the incident ion direction, elongate perpendicular to it or stay unchanged [6, 7]. It is important to mention that in the most of the studied cases authors have used SHI having S_e values exceeding S_e values of ions used in the present work and NPs were embedded in amorphous silica matrix.

In our previous work we have studied Ge or Ni/SiO_2 multilayer films obtained by magnetron sputtering deposition. In cases where standard thermal annealing is applied to such multilayer, Ge NPs are formed and distributed randomly in a Ge-rich layer by diffusion mediated nucleation [8–10]. However if irradiation is applied before annealing, the Ge NPs formed during annealing show long range ordering and their sizes, distances, and arrangement type depend both on the irradiation parameters and the multilayer properties [11]. Ordering was explained by two ion beam properties: ion electronic stopping (S_e) and the efficiency to transfer

Table 1. Ion beams used for the irradiation together with their electronic (S_e) and nuclear (S_n) stopping power values for pure alumina matrix. E denotes the energy of the used ions and $\Delta T\,(r = 0)$ is the temperature increase in the center of the ion track caused by the MeV heavy ion passage. In all cases, irradiation was performed at RT (~300 K).

Ion	E (MeV)	S_e (keV nm^{-1})	S_n (keV nm^{-1})	ΔT $(r = 0)$ (K)
^{16}O	2	1.89	0.02	1680
^{16}O	3	2.08	0.01	1950
^{28}Si	15	4.39	0.01	4060
^{132}Xe	0.4	0.67	2.67	6710

deposited energy from the electron to the phonon system. To better understand the effects that ions induce in the material, analytical thermal spike model (ATSM) [12] was applied to calculate temperature profiles inside the ion tracks and to explain the observed structural properties of the irradiated films. The similar effect was also seen for Ni+ SiO_2 system, although small Ni NPs were already formed during the multilayer deposition.

Contrary to that, in Ge or Ni/Al_2O_3 multilayer films, body centered tetragonal (BCT) lattice of Ge or Ni NPs is formed already during magnetron sputtering deposition as is described in our previous work [13, 14]. In the present work we wanted to study ion beam induced effects on NPs in alumina matrix. As will be shown, the used MeV heavy ions do not change in any way the shape, size or distances between existing NPs. However, from the grazing incidence small angle x-ray scattering (GISAXS) measurements can be clearly seen that the entire NP lattice is tilted by an angle $\Delta\Phi$ in cases where irradiation is performed under some angle φ_{irr} with respect to the sample surface ($\varphi_{irr} < 90°$). Dependence of the tilt angle on primary ion energy, incident angle and ion fluence will be discussed. The obtained results are important for the controlled manipulation of three-dimensional NP lattices in amorphous matrices. Additionally, the results show that the tilt angle of the NP lattice in alumina matrix increases nearly linearly with the ion beam fluence and irradiation angle.

2. Experimental

Multilayer films containing Ge NPs were produced by magnetron sputtering deposition of 20(Ge+Al_2O_3)/ Al_2O_3 bi-layers on Si(111) or fused silica substrate. The deposition was performed at room temperature (RT) and details about the deposition can be found in [13]. The total thickness of the deposited multilayers was around 100 nm and both the Ge NPs and the alumina matrix were amorphous after the deposition. To obtain metal NPs, 10 alternating Al_2O_3/Ni bi-layers were prepared also by magnetron sputtering deposition on Si(111) or fused silica substrates. The total thickness of the alumina-based film was around 130 nm. After deposition, the Ni NPs were already crystalline [14], while the alumina matrix was amorphous as for the case of Ge NPs. The multilayers were then irradiated at RT by various ions (2 MeV O, 3 MeV O, 15 MeV Si, 0.4 MeV Xe) at one of the three ion fluences ($D_1 = 5 \times 10^{14}$, $D_2 = 1 \times 10^{15}$ or $D_3 = 2 \times 10^{15}$ ions cm^{-2}) and one of the three incidence angles with respect to the multilayer surface ($\varphi_{irr} = 30°, 60°$ or $90°$). When calculating ion fluences on the sample it was always taken into account that due to the different φ_{irr} different area at the sample surface was irradiated and therefore different number of incident ions are needed to obtain the same ion fluence. Irradiations with 2 and 3 MeV O and 15 MeV Si ions were performed at the Ruđer Bošković Institute, while irradiation with 0.4 MeV Xe ions was done at the Helmholtz-Zentrum Dresden-Rossendorf. Ion beams used for the irradiation together with their electronic (S_e) and nuclear (S_n) stopping power values calculated using SRIM 2008 code [15] are shown in table 1. The stopping powers were calculated for a pure alumina matrix, neglecting the contributions of Ge or Ni on the calculated parameters. This was possible while the atomic concentration of Ge or Ni in the multilayer film was 4% or 9%, respectively. Atomic concentrations were determined using time-of-flight elastic recoil detection analysis (TOF-ERDA) with 23 MeV ^{127}I ions and spectrometer positioned at 37.5° [16]. The energy of the used O and Si ions was high enough to ensure that ions interact with the multilayer only by energy transfer through the electronic stopping S_e, which is not changing very much throughout the entire multilayer. Elastic collisions with the nuclei in the target material (nuclear stopping power S_n) that become dominant near the end of the ion range can be neglected. However this was not the case for 0.4 MeV Xe ions where from the start S_n was larger than S_e and ions got completely stopped in the multilayer part close to the substrate (the penetration range of 0.4 MeV Xe ions in pure alumina is ~120 nm). It is important to mention that S_n is practically constant throughout the first 100 nm of alumina.

The internal structure of the multilayer films was investigated by GISAXS and by scanning transmission electron microscopy (STEM) measurements. GISAXS measurements were performed at the Synchrotron

Elettra, Trieste, using the SAXS beam line and photons with the energy of 8 keV. The scattered photons were detected with a 2D image plate detector. From the GISAXS spectra information about the NP shapes, sizes, size distributions, arrangement type and separation among them can be obtained [1]. The big advantage of the GISAXS method is that no special sample preparation is needed, measurements are fast and yield experimental data with excellent statistics (e.g. 10^{12} NPs in the irradiated volume can be simultaneously analyzed). The GISAXS technique is especially suitable for the analysis of irradiation effects, because irradiation-induced structural changes in the films cause the appearance of strong correlation maxima (Bragg sheets) in their GISAXS maps. STEM measurements were performed using a JEOL 2010 F microscope, operated at 200 kV and equipped with a field-emission gun and a high-angle annular dark-field detector (HAADF) for Z-contrast imaging.

Passing through the material, MeV heavy ions slow down mostly due to the inelastic scattering on electrons. The lost kinetic energy is deposited in the surrounding material, causing a temporary increase of the temperature within a cylindrical region around the ion trajectory called the ion track [12, 17–19]. The width of the ion track represents the region where increase of the temperature is high enough to cause significant changes in the material. To evaluate the temperature increases within the ion track ATSM model was employed [11, 12, 20] and initial temperature width parameter (a_0) as well as the fraction of the deposited energy S_e transferred into the energy of the thermal spike (g) were estimated. At present, the ATSM parameters can be estimated only from the experimental data for a-SiO$_2$ [21–24]. From our analysis, following the procedure described in [12], we deduce that for a-SiO$_2$ $a_0 = 2.8 \pm 0.2$ nm and $g = 0.50 \pm 0.05$ for low velocity irradiation like the one used in the present work. The ATSM parameters a_0 and g are unknown for amorphous alumina because there are no experimental data reported in the literature known to us on ion tracks in that material and therefore the same values of a_0 and g found for the amorphous silica system were used [25]. Furthermore, the properties of amorphous materials differ from those of crystalline materials. Hence we employ measured value for the amorphous alumina density $\rho = 3$ g cm^{-3} deduced from the TOF-ERDA (giving us the number of atoms per cm^2) and GISAXS (providing us the total thickness of the film), and we estimate reduction of 20% in the melting temperature [26, 27] compared to the sapphire because the thermal properties of the amorphous alumina are also not known at present [28]. To calculate the temperature increase for 0.4 MeV Xe ion irradiation where nuclear stopping dominates, we use the ATSM parameters of $a_0 = 2.8 \pm 0.2$ nm and $g = 1$, based on the analysis of the data from [22]. This is also in line with the observation of Szenes that up to 90% of the nuclear stopping power might contribute to the thermal spike [29]. The calculated temperature increases in the center of the ion track caused by the ion beam passage $\Delta T(r = 0)$ are displayed in table 1. Taking into account that estimated melting point of amorphous alumina is at ~1880 K, we can see that for all used ions temperature in the center of the track after ion passage is 300 K $+ \Delta T(r = 0)$ which is in all cases higher than the estimated melting temperature.

3. Results and discussion

Contrary to the case of (Ge+SiO$_2$)/SiO$_2$ multilayers where no visible Ge clustering can be seen if magnetron sputtering deposition is performed at the RT, in the case of (Ge+Al$_2$O$_3$)/Al$_2$O$_3$ multilayers, amorphous Ge NPs always form during the magnetron sputtering deposition regardless if the deposition is performed at RT or at a slightly elevated temperature [13, 30]. After additional post-annealing at ~1000 K, amorphous Ge NPs crystallize. More about the properties of Ge NP lattices in amorphous alumina can be found in [30].

Here we will focus only on the effects caused by the MeV heavy ion passage through such film containing a BCT lattice of Ge NPs in alumina matrix. Figure 1(a) shows GISAXS map of a multilayer film before the ion irradiation. The formed Ge NPs are ordered in a regular NP lattice due to the self-assembled growth regime. More specifically, they are ordered in NP lattices with BCT structure, similarly to the ordering of atoms in a crystalline lattice. A very similar structure, but with tilted lattice is found after the irradiation (figure 1(b)). Such regular ordering induces appearance of diffraction (Bragg) spots and sheets in the GISAXS maps of the films. (The spots are indicated by circles and lines in figures 1(a) and (b).) These spots are related to Ge NP ordering mainly, while the sheets are related also to the correlated interface roughness of the multilayer. The self-assembled growth is a consequence of the nucleation during the film growth combined with the surface morphology effects [30]. From figures 1(a) and (b) is evident that the Bragg spots in the GISAXS maps are symmetrical for the as-grown film, while they appear with the same structure but tilted for the angle $\Delta\Phi$ after film irradiation with 2 MeV O ions under $\varphi_{irr} = 60°$. This tilt of the Bragg spots strongly indicates the tilt of the entire NP lattice. Therefore, the numerical analysis of the GISAXS maps has been performed in order to get the real values of the size and arrangement parameters. For the analysis we have used the paracrystal model given in [31]. The BCT ordering of NPs is assumed and ellipsoidal shape with the characteristic radii R_L and R_V in directions parallel and perpendicular to the surface respectively. The in-plane separation of the NPs is found to
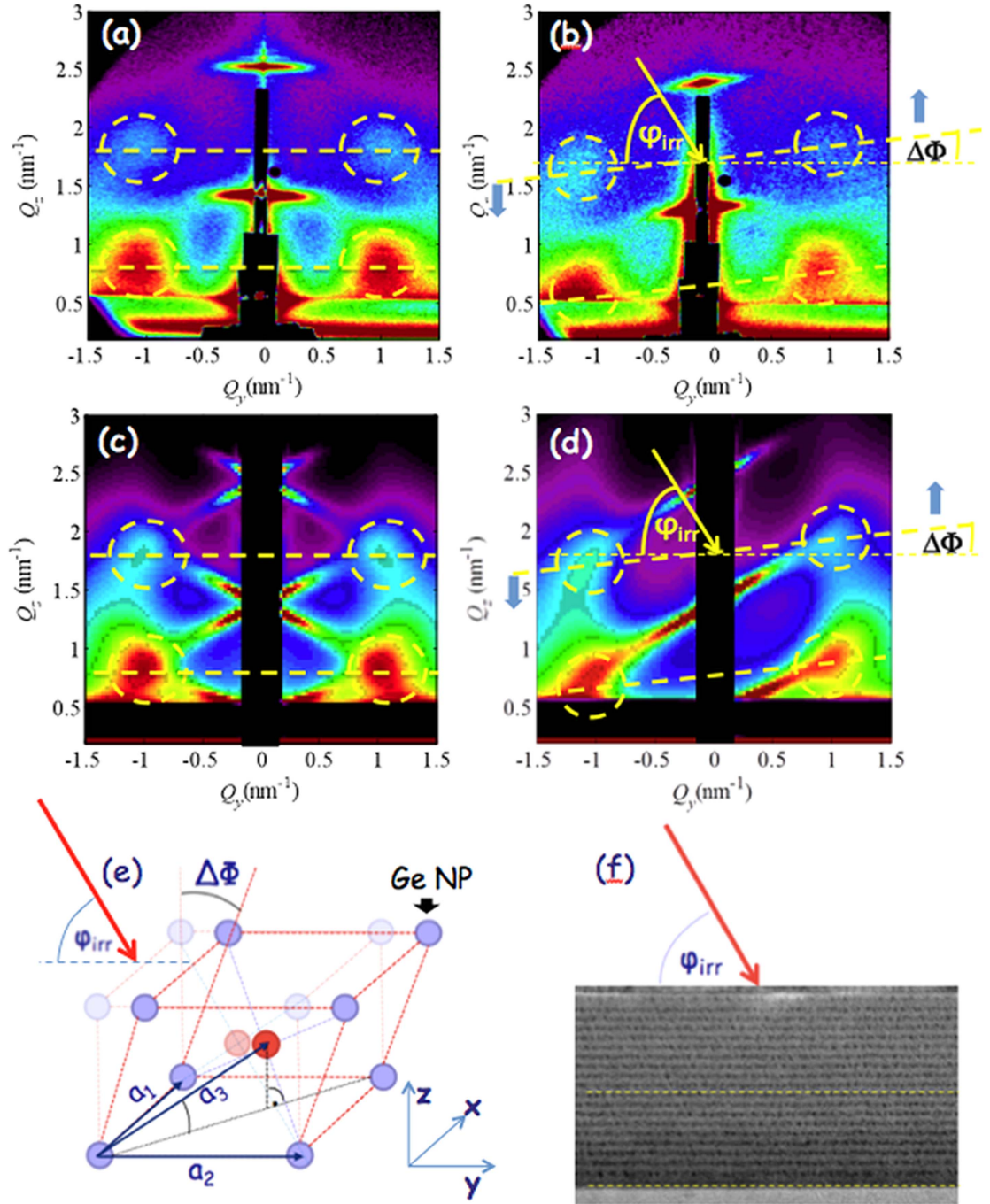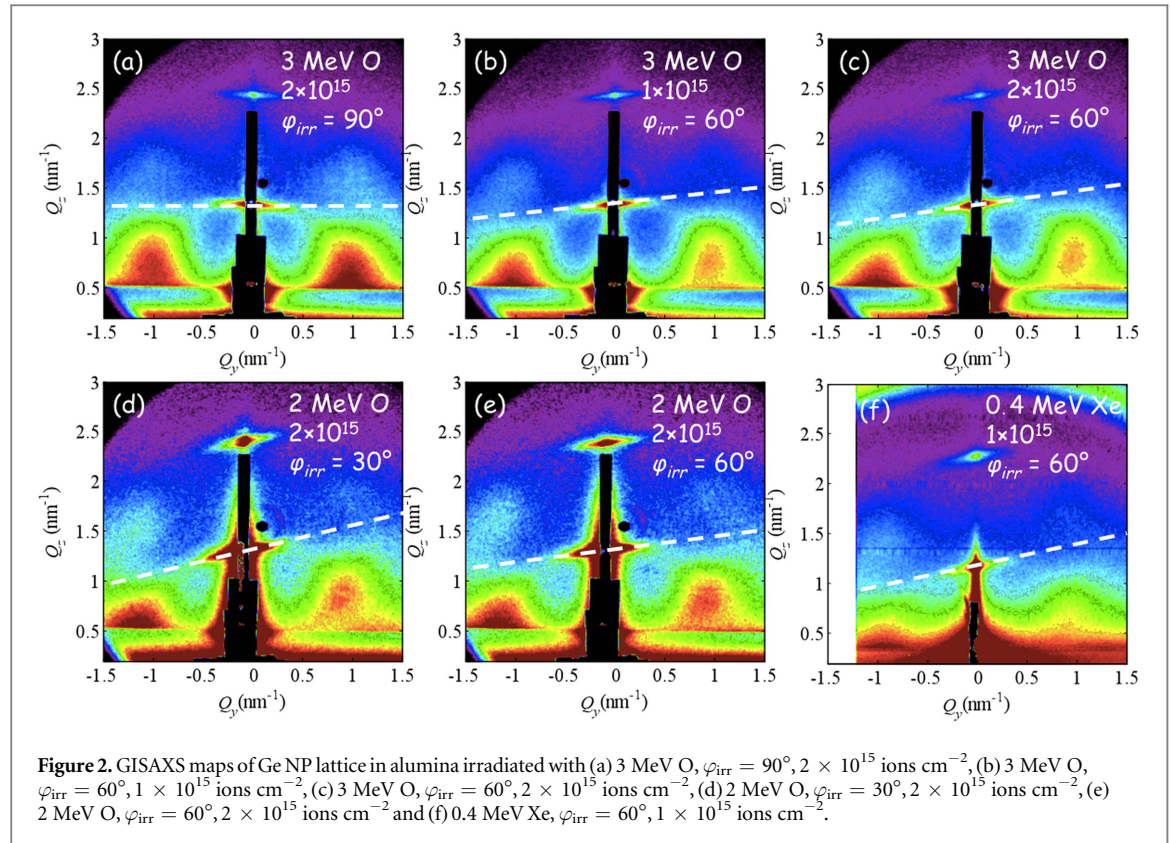
Figure 1. GISAXS maps of Ge NP lattice deposited at RT (a) as-grown and (b) irradiated with 2 MeV O ions under $\varphi_{irr} = 60°$. (c), (d) Simulations of the GISAXS maps shown in panels (a) and (b) respectively, obtained by using the results of their numerical analysis. (e) Model of Ge NP ordering in a NP lattice defined by basis vectors $\boldsymbol{a_1}-\boldsymbol{a_3}$. Ions induce a distortion of the BCT NP lattice by the angle $\triangle\Phi$. The coordinate system indicates the geometry used in the experiment. (f) TEM image shows that after ion irradiation the layers in the multilayer remain parallel to the Si substrate surface.

be 5.6 nm, while the multilayer period is 5.3 nm. The GISAXS maps simulated by using the parameters obtained by fit are shown in figures 1(c) and (d). The numerical analysis and simulations reproduce well the intensity distributions for $Q_y > |0.5|\text{nm}^{-1}$ where the main contribution to GISAXS originates from NPs. However, the models do not take into account the interface roughness contribution which is partially related to the appearance of Bragg sheets centered at $Q_y = 0 \text{ nm}^{-1}$. Therefore, only the positions of the centers of the Bragg sheets are reproduced well in the simulations, while their tilt angle cannot be reproduced (for details please see [31]). The radii of the NP are found to be 0.65 nm. The same values are obtained for the GISAXS map of the irradiated film. The obtained values agree well with the TEM studies.

The ordering type of Ge NPs is demonstrated in figure 1(e). Basis vectors $\boldsymbol{a_1}-\boldsymbol{a_3}$ define the formed lattice ($\boldsymbol{a_1}$ is set along *x*, $\boldsymbol{a_2}$ along *y*). The regular ordering actually appears in domains that are randomly rotated around the

Figure 2. GISAXS maps of Ge NP lattice in alumina irradiated with (a) 3 MeV O, $\varphi_{irr} = 90°$, 2×10^{15} ions cm^{-2}, (b) 3 MeV O, $\varphi_{irr} = 60°$, 1×10^{15} ions cm^{-2}, (c) 3 MeV O, $\varphi_{irr} = 60°$, 2×10^{15} ions cm^{-2}, (d) 2 MeV O, $\varphi_{irr} = 30°$, 2×10^{15} ions cm^{-2}, (e) 2 MeV O, $\varphi_{irr} = 60°$, 2×10^{15} ions cm^{-2} and (f) 0.4 MeV Xe, $\varphi_{irr} = 60°$, 1×10^{15} ions cm^{-2}.

normal to the surface (*z* axis). The main irradiation vector is in the *y–z* plane, while the GISAXS maps are measured with the probing x-ray beam set along *x* axis (perpendicular to the irradiation). It is important to mention that the layers within the multilayer remain parallel to the Si substrate surface after the ion beam irradiation, as visible from the TEM image displayed in figure 1(f).

The tilt angle $\Delta\Phi$ by which the NP lattice is distorted depends on the ion type, fluence and incidence angle and was observed for all used ions (O, Si and Xe ions) and all used ion energies. Figure 2(a) shows GISAXS map of Ge NP lattice irradiated with 3 MeV O ions under normal incidence. No inclination of Bragg spots or sheets can be seen. However, if the same sample is irradiated with two different fluences of 3 MeV O ions (figures 2(b) and (c)) under $\varphi_{irr} = 60°$, Bragg spots and sheets are inclined and slight increase of the tilt angle with the ion fluence can be seen. Similar effect is caused by the change of the irradiation angle as is visible from the figures 2(d) and (e) for case of 2 MeV O. Smaller irradiation angle with respect to the film surface causes the larger tilt of the NP lattice for the same applied fluence. Tilt of the Bragg spots and sheets can be seen also for sample irradiated with 0.4 MeV Xe ions (figure 2(f)), although in that case the ions interact with the layer mostly through the nuclear stopping and also they are completely stopped in the layer near the substrate. Here traces of the layer destruction can also be seen since the Bragg spots deriving from the NPs are not so clear as in case of the other used ions.

Similar to the case of Ge NPs, Ni NPs have a good ordering quality and form well-defined clusters with larger sizes in amorphous alumina matrix already in films deposited at RT. Generally, the metal clusters usually form in thin films regardless of the matrix composition already at RT, which is not the case for Ge. Additionally, the formed metal NPs are crystalline [14], while Ge clusters are always amorphous after deposition even for the higher deposition temperatures [9]. It was shown that the Ni particle size, separation and quality of ordering in amorphous alumina could be tuned by the deposition time of Ni-rich layers [30]. From the high-resolution TEM image of Ni NPs formed in alumina matrix (figure 3(a)) can be seen that the formed NPs have an almost spherical shape and uniform sizes. Structural measurements on the films performed by GISAXS have shown that Ni NPs are also forming a BCT lattice (figure 3(b)), as was observed for Ge NPs in alumina. This we attribute to a similar self-assembly process that is in both cases governed by the properties of the amorphous alumina matrix (in particular by its surface morphology). Again, irradiations with MeV ions under $\varphi_{irr} = 60°$ have caused a tilt of the NP lattice as shown in figure 3(c). Hence Ni NPs in alumina, which are well formed and crystalline after deposition, show the same behavior as Ge NPs in alumina.

It is important to mention that we have not observed any change of Ge or Ni NP shape or size after irradiation with ion beams regardless different melting temperatures of Ge (1211 K) and Ni (1728 K). Namely, GISAXS is very sensitive even to the small changes in the NP average shape and size. Any asymmetry in the
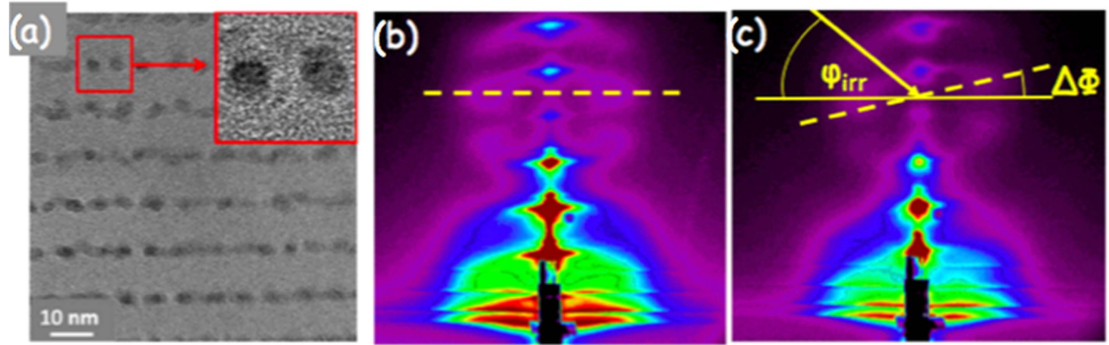
Figure 3. (a) High-resolution TEM image of a Ni NP lattice obtained by deposition of a (Ni+Al$_2$O$_3$)/Al$_2$O$_3$ multilayer film at RT. (b) GISAXS 2D image of the as deposited film giving us information about the NP sizes, distributions and ordering type (BCT). (c) After irradiation with 1×10^{15} at cm^{-2} 15 MeV Si ions under $\varphi_{irr} = 60°$ NP lattice is tilted for an angle $\Delta\Phi$ compared to the non-irradiated lattice.
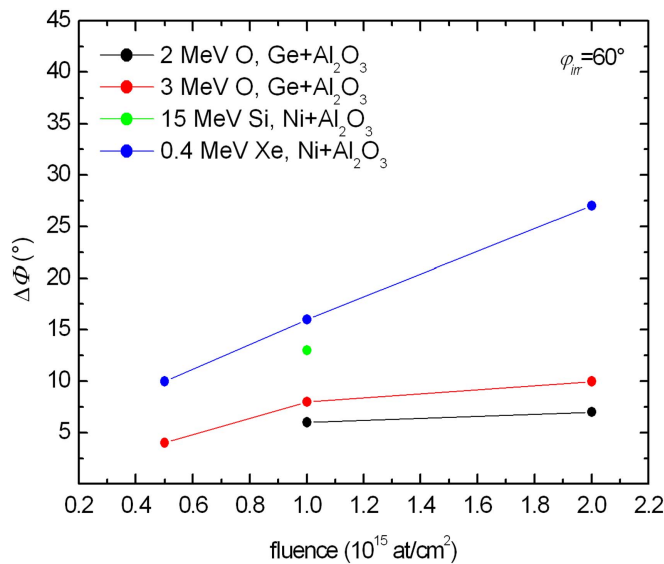

Figure 4. Dependence of the tilt angle $\Delta\Phi$ after irradiation of Ni and Ge NP lattices in amorphous alumina with different fluences of O, Si and Xe ions at the irradiation angle $\varphi_{irr} = 60°$.

average NP shape caused by the ion beam should cause asymmetrical contribution to the GISAXS intensity distribution via form factor, which is not observed. Therefore the changes, if present, are very small. One of the reasons for that can be size of the NPs, which is in our case below 5 nm. It can be seen from the literature [32] that ion beam shaping on NP in thin films depends also on NP dimension and that NPs smaller than about 8–10 nm remain spherical in shape.

The dependence of the NP lattice tilt angle after irradiation at $\varphi_{irr} = 60°$ of different multilayer types with different energies and fluences of MeV heavy ions is summarized in figure 4. From figure can be clearly seen that tilt angles in all cases increase with applied ion fluence. This dependence means that the shear (shift of the layers) increases with the number of ions that hit the sample. The relation between the irradiation angle φ_{irr} and the tilt angle $\Delta\Phi$ for Ge and Ni NPs in amorphous alumina matrix can be seen in figure 5. Again, a nearly linear dependence is observed for all ions as a function of the irradiation angle. Also, it can be clearly seen that for the same ion type and fluence (O ions, 2×10^{15} at cm^{-2}) the tilt of the NP lattice is larger for 3 MeV than for 2 MeV O ions. Thus, all irradiation parameters (irradiation angle, ion energy and fluence) can be used for the control of the NP lattice parameters and generally for the deformation of alumina-based material.

As NPs, regardless the type (Ge or Ni), retain their initial shape and in-layer separation they serve as a markers to quantify changes of the amorphous alumina matrix after irradiation with the MeV heavy ions. The shift of the layers is parallel to the film surface, however its value depends on the layer position within the multilayer. More precisely, the top layer shifts more in comparison to the bottom layers. This can be explained with a process known as irradiation induced anisotropic deformation or the ion-hammering effect [33–36]. The
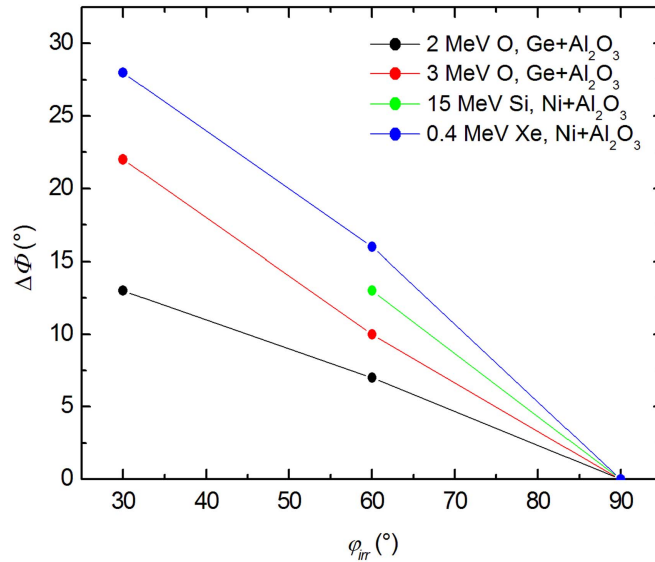
Figure 5. Relation between the irradiation angle φ_{irr} and the tilt angle $\Delta\Phi$ for Ge and Ni irradiated NP lattices in amorphous alumina. For 2 and 3 MeV O fluence was 2×10^{15} at cm^{-2}, for 15 MeV Si and 0.4 MeV Xe ions fluence was 1×10^{15} at cm^{-2}.
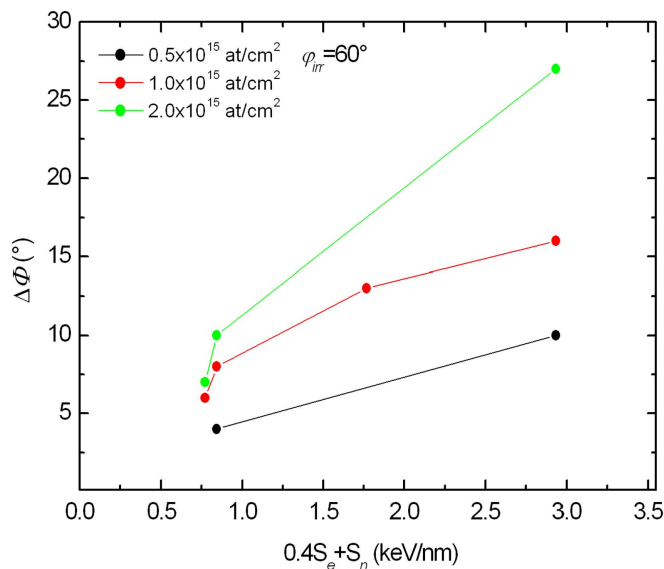

Figure 6. Dependence of the tilt angle $\Delta\Phi$ on the scaled stopping power $0.4S_e + S_n$ for NP lattices in amorphous alumina matrix for three different ion fluences 0.5×10^{15} at cm^{-2}, 1×10^{15} at cm^{-2} and 2×10^{15} at cm^{-2}. The irradiation was performed under $\varphi_{irr} = 60°$.

ion-hammering effect was observed in glassy and amorphous materials, which undergo irreversible deformation during irradiation with SHIs. The ion beam induced anisotropic plastic deformation is assumed to be directly related to the ion track formation since the deformation increases with the electronic energy loss [37, 38]. However, nuclear stopping can also play a role and should be taken into account since up to 90% of it might contribute to the thermal spike [29]. To take both contributions into account the dependence of the tilt angle $\Delta\Phi$ on the scaled electronic and nuclear stopping $0.4S_e + S_n$, which represents the energy density of the thermal spike, is shown on figure 6 for three different ion fluences 0.5×10^{15} at cm^{-2}, 1×10^{15} at cm^{-2} and 2×10^{15} at cm^{-2}. The irradiation angle was in all cases 60°. From the figure can be concluded that the plastic deformation increases with both, ion fluence and the scaled electronic and nuclear stopping.

The ion hammering model states that when the ion-track temperature exceeds a certain flow temperature, a complete shear stress relaxation takes place and upon fast cooling of the spike region, the strain increment associated with the stress relaxation freezes in. Thus the resulting strained track represents the mesoscopic defect responsible for the anisotropic deformation. Van Dillen *et al* have demonstrated that free standing silica particles expand perpendicular and contract parallel to the ion beam changing their shape from spherical to oblate

Figure 7. Plot of the deformation yield A versus the thermal spike energy density $0.4S_e + S_n$.
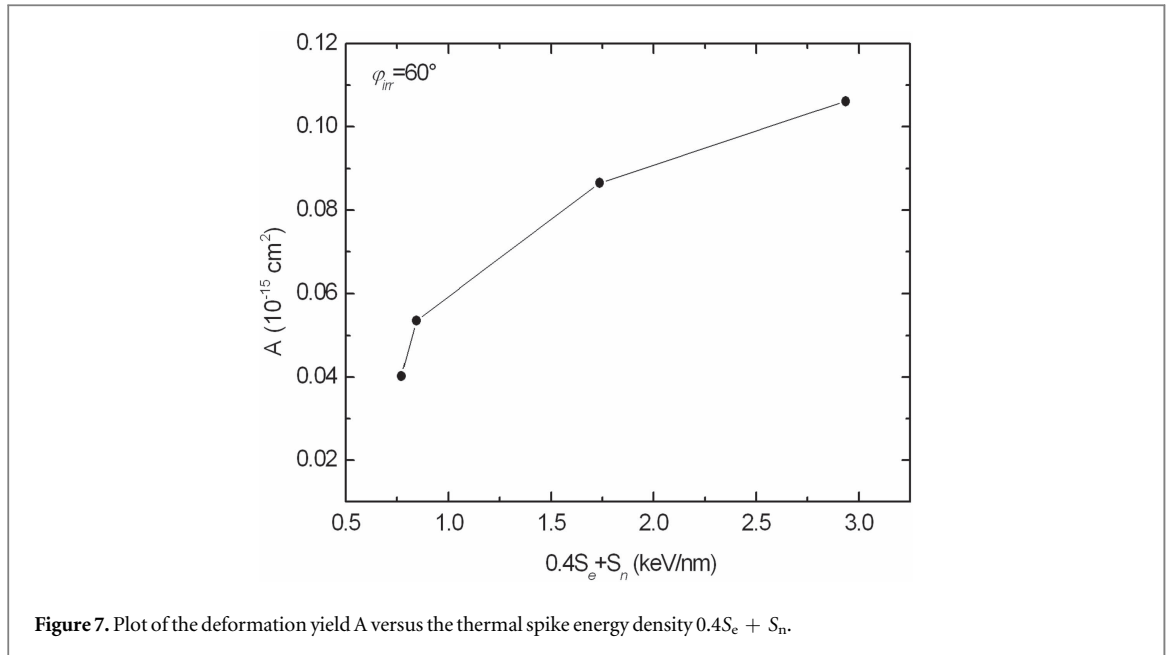
ellipsoidal [39, 40]. Several authors have shown that in case when thin metallic glass or amorphous film placed on the top of a crystalline substrate is irradiated with energetic ions under some angle, shear cannot be prevented by the substrate because of the traction-free surface so that the entire amorphous layer is sheared [41–43]. It is assumed that the amorphous layer thickness is much smaller then the range of the ions that pass through it so we can assume that electronic stopping power S_e is nearly constant throughout the layer and that ions stop deep inside the substrate. This plastic deformation was quantified by measuring directly the surface shift (Δx) and the compaction (Δz) of the irradiated part of the sample towards the non-irradiated part as a function of the ion fluence for different incident ions and energies (for an example please see figure 2 in [42]).

In our case the condition that layer thickness is much smaller than the range of the ions used for the irradiation is true for 2 MeV O, 3 MeV O and 15 MeV Si but not for 0.4 MeV Xe. Also, instead of measuring the surface shift Δx and the compaction Δz, with GISAXS we can measure directly the tilt angle $\Delta \Phi$ by which the entire NP lattice gets inclined. According to [41], in case of an amorphous thin film on a crystalline substrate, the strain tensor describing the ion hammering is not isotropic but contains a shear component in the ion beam direction and the shift of the irradiated part of the surface is equal to

$$\Delta x = 3YAd \sin(2\theta), \tag{1}$$

where A is deformation yield, d is amorphous layer thickness, θ is incident ion angle relative to the sample surface normal and Y is the ion fluence. In our case

$$\Delta x = \sin(\Delta \Phi)d \tag{2}$$

and from equations (1) and (2) we get

$$A = \frac{\sin(\Delta \Phi)}{3Y \sin(2\Theta)}, \tag{3}$$

where $\theta = 90° - \varphi_{irr}$. The deformation yield A depends on the specific material and on the temperature at which the ion irradiation was performed. The dependence of A on the irradiation temperature and stopping power S_e was measured for vitreous silica with 4 MeV and 340 MeV Xe ions with fluences $<10^{14}$ at cm^{-2} and different irradiation temperatures [44, 45]. Contrary to silica, for amorphous alumina no experimental data for deformation yields exist in the literature. Taking into account the measured data for all ions used in the present work and an ion fluence of 1×10^{15} at cm^{-2}, the dependence of the deformation yield A in amorphous alumina on the thermal spike energy density (evaluated as a scaled electronic and nuclear stopping $0.4S_e + S_n$) can be calculated and the result is displayed in figure 7.

While the ion hammering effect is generally related to the ion track formation (i.e. melting of the material upon ion impact), we have found that surprisingly low values of electronic stopping power are sufficient to induce this effect in amorphous alumina. Skuratov *et al* [46] irradiated crystalline Al_2O_3 with 167 MeV Xe ions and they have found that the threshold S_e for ion track formation in sapphire is around 10 keV nm^{-1}. This is in agreement with previous work on the threshold stopping power for amorphization of sapphire after high fluence irradiation [47–49]. However, in our case we see a shift of the NP lattices for all used ions and energies which have significantly lower values of S_e than 10 keV nm^{-1} as can be seen from table 1. One of the reasons can be that

amorphous alumina deposited by magnetron sputtering is much more sensitive to MeV heavy ions than sapphire. Furthermore, the ion fluences used in the present work are higher than the ones used in previous studies on anisotropic deformation ($\sim 10^{13}$ at cm^{-2}). Audouard *et al* [50] have shown that for low values of S_e, overlapping ion impacts (i.e. higher fluences) can drive anisotropic deformation as well. The explanation of this overlapping effect is, that at stopping power values, which are subcritical for anisotropic growth, the first impact does not cause any growth but induces structural modifications of the material, and only subsequent ion impacts on the modified material drive the growth process. As shown in figure 3 in [50], this so called 'two hit model' can explain the substantial lowering of the threshold for the ion hammering effect. To verify that this mechanism is indeed responsible for the observed anisotropical deformation at higher fluences, we plan to investigate possible anisotropic flow at lower ion fluences. Then, by measuring the kinetics of the observed ion hammering effect, it would be possible to evaluate both the ion track diameters and number of track overlaps needed to drive the process.

4. Conclusions

The effects produced by irradiation of regularly ordered NP lattices embedded in amorphous alumina with MeV heavy ions were studied using the GISAXS method. From the GISAXS intensity maps can be concluded that the used MeV heavy ions do not change the NPs as concerning their sizes, shapes or the distances among them. However, it can be clearly seen that the entire NP lattice gets tilted in the direction parallel to the sample surface. It was found that the tilt angle depends on the incident ion energy, type, and applied ion fluence. A nearly linear increase of the tilt angle with the ion fluence and irradiation angle was found. For the first time, the deformation yield A in amorphous alumina was determined for high ion fluences and irradiation performed at the RT. It can be concluded that plastic deformation in amorphous alumina can be detected for stopping power values of 1.9 keV nm^{-1}, which is significantly lower than the threshold for ion track formation in sapphire (10 keV nm^{-1}). Last but not least, it was demonstrated that GISAXS is a very efficient method to study MeV heavy ion induced modification of materials with embedded NP lattices.

Acknowledgments

References

[1] Gramotnev D K and Bozhevolnyi S I 2010 *Nat. Photon.* **4** 83
[2] Barnes W L, Dereux A and Ebbesen T W 2003 *Nature* **424** 824
[3] Jabbour G E and Doderer D 2010 *Nat. Photon.* **4** 604
[4] Ladd T D, Jelezko F, Laflamme R, Nakamura Y, Monroe C and O'Brien J L 2010 *Nature* **464** 45
[5] Ridgway M C *et al* 2011 *Phys. Rev. Lett.* **106** 095505
[6] Schmidt B, Heinig K H, Mucklih and Akhmadaliev C 2009 *Nucl. Instrum. Methods* B **267** 1345
[7] Araujo L L, Giulian R, Sprouster D J, Schnohr C S, Llewellyn D J, Johannessen B, Byrne A P and Ridgway M C 2012 *Phys. Rev.* B **85** 235417
[8] Buljan M, Bogdanović Radović I, Karlušić M, Desnica U V, Radić N, Jakšić M, Salamon K, Dražić G, Bernstorff S and Holy V 2011 *Phys. Rev.* B **84** 155312
[9] Buljan M, Desnica U V, Ivanda M, Radić N, Dubček P, Dražić G, Salamon K, Bernstorff S and Holy V 2009 *Phys. Rev.* B **79** 035310
[10] Buljan M, Desnica U V, Dražić G, Ivanda M, Radić N, Dubček P, Salamon K, Bernstorff S and Holy V 2009 *Nanotechnology* **20** 085612
[11] Bogdanović Radović I, Buljan M, Karlušić M, Skukan N, Božičević I, Jakšić M, Radić N, Dražič G and Berstorff S 2012 *Phys. Rev.* B **86** 165316
[12] Szenes G 1995 *Phys. Rev.* B **51** 8026
[13] Buljan M *et al* 2013 *J. Nanopart. Res.* **15** 1485
[14] Jerčinović M *et al* 2014 *J Nanopart. Res.* **16** 2296
[15] Ziegler J J F 2004 *Nucl. Instrum. Methods* B **219** 1027
[16] Siketić Z, Bogdanović Radović I, Jakšić M and Skukan N 2010 *Rev. Sci. Instrum.* **81** 033305
[17] Toulemonde M, Trautmann C, Balanzat E, Hjort K and Weidinger A 2004 *Nucl. Instrum. Methods* B **216** 1
[18] Fleischer L R, Price P B and Walker R M 1975 *Nuclear Tracks in Solids: Principles and Applications* (Berkeley, CA: University of California Press)
[19] Brongersma M L, Snoeks E and Polman A 1997 *Appl. Phys. Lett.* **71** 1628
[20] Buljan M, Karlušić M, Bogdanović Radović I, Jakšić M, Salamon K, Bernstorff S and Radić N 2012 *Appl. Phys. Lett.* **101** 103112
[21] Kluth P *et al* 2008 *Phys. Rev. Lett.* **101** 175503
[22] Toulemonde M, Webber W J, Li G, Shutthanandan V, Kluth P, Yang T, Wang Y and Zhang Y 2011 *Phys. Rev.* B **83** 054106

[23] Rotaru C, Pawlak F, Khalfaoui N, Dufour C, Perrière J, Laurent A, Stoquert J P, Lebius H and Toulemonde M *Nucl. Instrum. Methods* B **272** 9
[24] Benyagoub A and Toulemonde M 2015 *J. Mater. Res.* **30** 1529
[25] Rymzhanov R A, Medvedev N A and Volkov A E 2015 *Nucl. Instrum. Methods* B **354** 292
[26] Toulemonde M, Dufour C and Paumier E 1992 *Phys. Rev.* B **46** 14362
[27] Donovan E P, Spaepen F, Turnbull D, Poate J M and Jacobson D C 1985 *J. Appl. Phys.* **57** 1795
[28] Tavakoli A H, Maram P S, Widgeon S J, Rufner J, van Benthem K, Ushakov S, Sen S and Navrotsky A 2013 *J. Phys. Chem.* C **117** 17123
[29] Szenes G 2002 *Nucl. Instrum. Methods* B **191** 27
[30] Buljan M *et al* 2013 *J. Appl. Cryst.* **46** 1490
[31] Buljan M, Radić N, Bernstorff S, Dražić G, Bogdanović-Radović I and Holý V 2012 *Acta Cryst.* A **68** 124
[32] Rizza G 2015 *J. Phys.: Conf. Ser.* **629** 012005
[33] Klaumünzer S and Schumacher G 1983 *Phys. Rev. Lett.* **51** 1987
[34] Klaumünzer S 2004 *Nucl. Instrum. Methods* B **215** 345
[35] Klaumünzer S, Hou M D and Schumacher G 1986 *Phys. Rev. Lett.* **57** 850–3
[36] Klaumünzer S 1992 *Mater. Sci. Forum* **97–99** 623
[37] Trinkaus H and Ryazanov A I 1995 *Phys. Rev. Lett.* **74** 5072
[38] Trinkaus H 1998 *Nucl. Instrum. Methods* B **146** 204
[39] Snoeks E, van Blaaderen A, van Dillen T, van Kats C M, Brongersma M L and Polman A 2000 *Adv. Mater. Weinheim, Ger.* **12** 1511
[40] van Dillen T, Snoeks E, Fukarek W, van Kats C M, Velikov K P, van Blaaderen A and Polman A 2001 *Nucl. Instrum. Methods* B **175–177** 350
[41] Gutzman A and Klaumünzer S 1997 *Nucl. Instrum. Methods* B **127/128** 12
[42] Hedler A, Klaumünzer S L and Wesch W 2004 *Nat. Mater.* **3** 804
[43] Hedler A, Klaumünzer S L and Wesch W 2006 *Nucl. Instrum. Methods* B **242** 85
[44] Benyagoub A and Klaumünzer S 1993 *Radiat. Eff. Defects Solids* **126** 105
[45] Brongersma M L, Snoeks E, van Dillen T and Polman A 2000 *J. Appl. Phys.* **88** 59
[46] Skuratov V A, O'Connell J, Kirilkin N S and Neethling J 2014 *Nucl. Instrum. Methods* B **326** 223
[47] Aruga T, Katano Y, Ohmichi T, Okayasu and Kazumata Y 2000 *Nucl. Instrum. Methods* B **166** 913
[48] Szenes G 2005 *J. Nucl. Mater.* **336** 81
[49] Szenes G 2013 *Nucl. Instrum. Methods* B **312** 118
[50] Audouard A, Dural J, Toulemonde M, Lovas A, Szenes G and Thome L 1996 *Phys. Rev.* B **54** 15690